AAAS

Science

28 MAY 2026

FINDING HOME

Liver macrophages guide pigeons on cloudy days **pp. 919 & 985**

ANIMAL NAVIGATION

Homing pigeon navigation relies on superparamagnetic macrophages under overcast conditions

Clivia Lisowski[1]*, Michael Quetting[2], Daniela Klaus[1], Lisa Lazarevski[1], Lea Seep[3], Maximilian Germer[1], Jian Li[1], Inge Müller[2], Daniel Zuniga[2], Wolfgang Fiedler[2], Dina K. N. Dechmann[2], Kasper Thorup[2,4], Jan Hasenauer[3], Lars Fester[5], Stefanie Kuerten[5], Michael Farle[6], Ulf Wiedwald[6], Martin Wikelski[2,7]*†, Christian Kurts[1,8]*†

Birds use a variety of navigational strategies, including the geomagnetic field, especially when other cues are not available, such as under overcast or nocturnal conditions. Magnetite particles in the beak, cryptochromes in the eye, cellular ion-channel alterations, and changes in the vestibular system have been proposed to explain magnetoreception, but the exact mechanisms remain debated. Here, we used physical, morphological, functional, and genomic assays to identify the presence of superparamagnetic macrophages in the liver. We found that after macrophage depletion, pigeons flying under overcast conditions lacked their usual orientation capabilities. Orientation was unimpaired in birds without macrophages when the sun was visible, suggesting that this was their primary cue. We propose that in homing pigeons, superparamagnetic macrophages in the liver are required for finding magnetic direction.

For many animals, the ability to determine their position on the globe and to maintain the correct course toward a target destination, known as navigation, is essential for survival (*1*, *2*). Field studies show that many species rely on magnetic orientation when other senses, such as vision, are limited (*3*, *4*). Birds have long provided an excellent model system for studying navigation. For example, songbirds migrating at night or under overcast skies can maintain a magnetically calibrated flight direction, set at sunset, over hundreds of kilometers (*5*, *6*). Pigeons use visual landmarks and/or environmental odors to determine their position and may also use a magnetic map (*7*). To keep a chosen course, birds use either a sun compass or a magnetic compass, which might operate independently. Unlike other vertebrate sensory systems with well-defined receptor organs (*8*), the mechanisms of magnetoreception have remained elusive and widely debated despite decades of intensive research (*9*–*15*).

Three principal mechanisms have so far been proposed to explain magnetoreception. The first is chemical magnetoreception via cryptochromes in the avian visual system (*16*–*18*). According to this theory, light-induced radical-pair reactions in cryptochromes provide sufficient activation energy to generate a magnetic-direction signal, allowing birds to "see" the magnetic field superimposed onto their visual scene (*19*). However, because cryptochromes are light-dependent, this mechanism cannot readily account for navigation in complete darkness. Moreover, the cryptochrome hypothesis has proven difficult to reproduce experimentally, and there is limited evidence for sustained magnetic navigation under natural dark conditions. Behavioral assays such as the Emlen funnel, a confinement device to study birds' migratory orientation by observing nocturnal restlessness and collecting foot scratches on a lined floor (*20*), do not fully recapitulate natural environments and are prone to interexperimenter variability (*21*), further complicating interpretation.

The second hypothesis posits that ferric iron (Fe^{3+}) or magnetite (Fe_3O_4) particles in cells of the upper beak align with Earth's magnetic field and may relay directional information via the trigeminal nerve (*10*, *22*). The third, more theoretical, model suggests that changes in magnetic fields may influence ion-channel activity or membrane dynamics, but neither the responsible cell types nor the neural pathways involved have been identified (*23*). Along these lines, a recent study identified neuronal activity in vestibular and pallial regions of pigeon brain after artificial magnetic stimulation (*24*), suggesting that these sites might also be involved in processing magnetosensory information. Although that study did not identify the underlying molecular mechanism and requires validation of in vivo relevance for navigation behavior, it supports the existence of light-independent magnetoreception and suggests possible candidate brain regions. Overall, none of these hypotheses fully explains magnetoreception, and key mechanistic gaps remain.

We previously reported that splenic red pulp macrophages in mice and humans are intrinsically superparamagnetic (*25*). This is due to their function of degrading damaged or aged erythrocytes, which results in the liberation of iron from hemoglobin; this iron is stored within these macrophages as ferritin, a protein complex that sequesters iron in nontoxic form (*26*, *27*). These dynamic, spherical protein nanocages can store up to 4500 iron atoms in a mineralized form and exist as soluble cytoplasmic proteins or are associated with vesicular compartments, such as lysosomes (*28*, *29*). It is unknown whether these magnetic properties are involved in magnetoreception.

Results

Pigeon liver tissue has superparamagnetic properties

To test for tissues with magnetic properties in pigeons, we screened their organs (liver, spleen, muscle, and inner and outer beak) by vibrating sample magnetometry (VSM). This revealed a magnetic blocking effect at a blocking temperature (T_B) of 12 K for liver and spleen (Fig. 1A), whereas muscle tissue and inner and outer beak showed increased magnetization only below 50 K (Fig. 1B, note the different scales). The superparamagnetic response of muscle and beak may have arisen from the sum of various types of unpaired electrons (Langevin paramagnetism), whereas in pigeon liver and spleen, this was overlaid by much stronger ferrimagnetic signals. Figure 1C shows a field-dependent magnetization of liver tissue. After subtracting a strong diamagnetic background, the saturation magnetization (M_S) decreased markedly between 2 and 30 K, resulting in a M_S of 0.024 ampere–square meters per kilogram ($A{\cdot}m^2\,kg^{-1}$) at $T = 2$ K. Such M_S cannot arise from paramagnets (here ferric iron) because their response would be strictly linear at magnetic induction (B) = 9 T and $T = 30$ K following the Brillouin function. The coercive field $\mu_0 H_C$ decreased from 67 mT at $T = 2$ K to zero above T_B (Fig. 1C). These signals were similar to the temperature- and field-dependent behavior described in highly purified ferritin nanoparticles from horse spleen (M_S = 0.83 $A{\cdot}m^2\,kg^{-1}$) (*30*) or in macrophages isolated by magnetic-activated cell sorting (MACS) from murine spleens ($M_S = 0.067\ A{\cdot}m^2\,kg^{-1}$) (*25*). The higher magnetization of purified ferritin (>30-fold) from horse spleen or isolated macrophages from murine spleen (nearly threefold) compared with that from pigeon liver tissue was likely due to the lower concentration

[1]Institute for Molecular Medicine and Experimental Immunology, University of Bonn and University Hospital Bonn, Bonn, Germany. [2]Department of Migration, Max Planck Institute of Animal Behavior, Radolfzell, Germany. [3]Computational Biology, Life and Medical Sciences (LIMES) Institute and Bonn Center for Mathematical Life Sciences, University of Bonn, Bonn, Germany. [4]Center for Macroecology, Evolution and Climate, GLOBE Institute, University of Copenhagen, Universitetsparken 15, Copenhagen, Denmark. [5]Institute of Neuroanatomy, University of Bonn and University Hospital Bonn, Bonn, Germany. [6]Faculty of Physics and Center for Nanointegration Duisburg-Essen, University of Duisburg-Essen, Duisburg, Germany. [7]Department of Biology, University of Konstanz, Konstanz, Germany. [8]Peter Doherty Institute of Infection and Immunology, University of Melbourne, Melbourne, VIC, Australia. ***Corresponding author. Email: cliso@uni-bonn.de (C.L.); ckurts@uni-bonn.de (C.K.); wikelski@ab.mpg.de (M.W.)** †These authors contributed equally to this work.

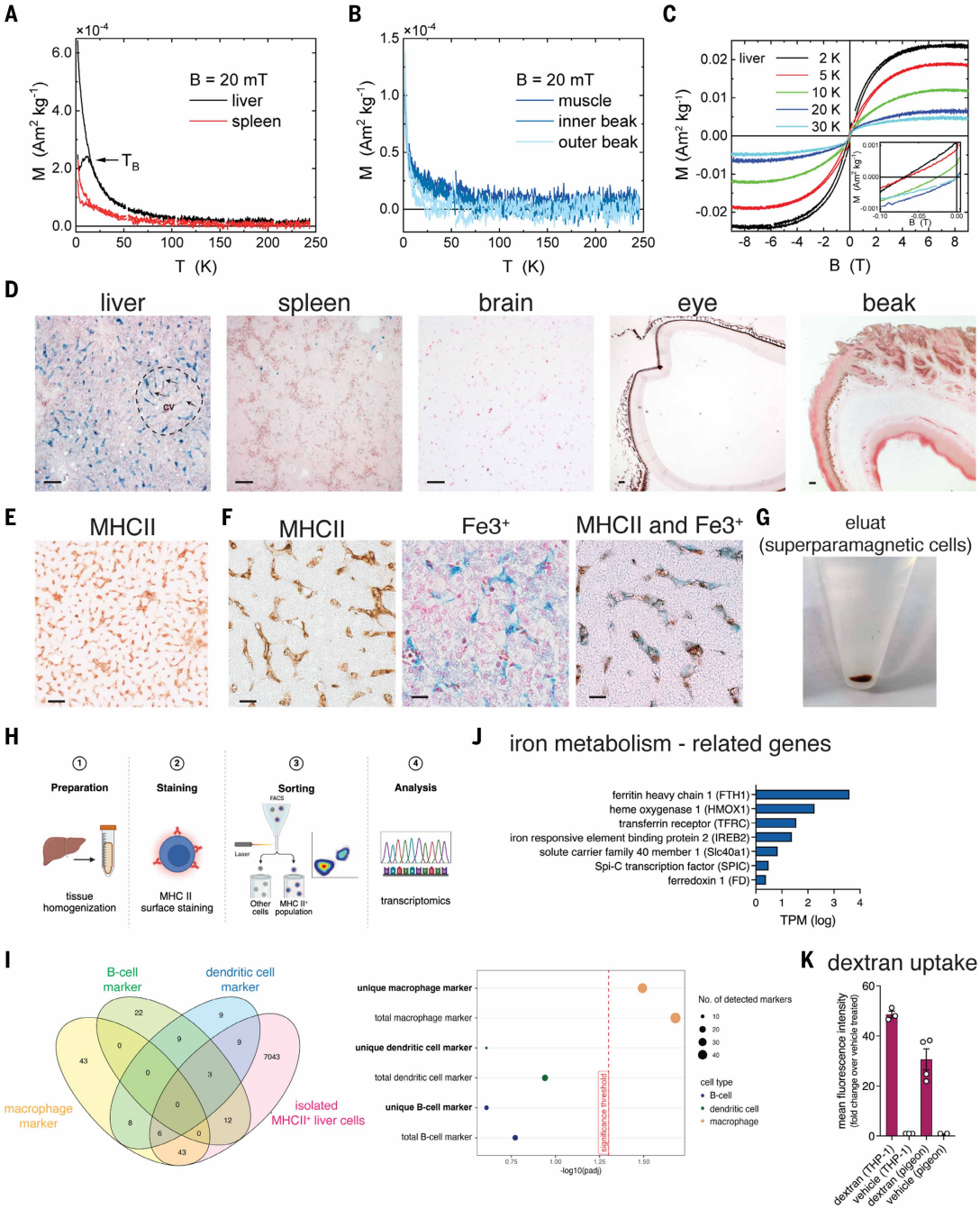

Fig. 1. Pigeon liver tissue exhibits superparamagnetic properties and contains iron-positive MHC II$^+$ macrophages. (**A**) Temperature-dependent magnetization according to the zero-field-cooling (ZFC) and field-cooling (FC) protocols of pigeon liver and spleen at $B = 20$ mT. (**B**) Temperature-dependent magnetization of muscle and the inner and outer beak. All curves start at a lower magnetization value after ZFC to $T = 2$ K. Liver and spleen samples exhibit a peak at the blocking temperature $T_B = 12$ K, whereas the magnetic responses of the muscle and inner and outer beak samples are independent of ZFC or FC. (**C**) Field-dependent magnetization at temperatures of 5 to 30 K of liver after the subtraction of diamagnetic slopes. The ferrimagnetic contribution saturates in inductions at B greater than ±6 T for all temperatures. For $T = 2$, 5, and 10 K, hysteresis loops are obtained, indicating long-range magnetic order. The inset shows a magnification of the first branch of hysteresis at a higher point density. The coercive field $\mu_0 H_C$ is read from the zero crossing of the magnetization. (**D**) Representative histological images of ferric iron (Fe^{3+}) staining in different organs isolated from rock pigeon (*C. livia*). Scale bars for liver, spleen, and brain are 100 μm; scale bars for beak and eye are 10 μm. The dashed line in the liver panel indicates a liver lobule with a central vein (CV); the arrows indicate sinosoids. (**E**) Representative histological image of MHC II staining in liver tissue. Scale bar is 100 μm. (**F**) Representative histological images of MHC II$^+$, Fe^{3+}, and combined staining of liver tissue. Scale bar is 50 μm. (**G**) Representative photo of hepatic cells isolated over a magnetic column. (**H**) Experimental setup for the sorting and sequencing of superparamagnetic liver cells. (**I**) Isolated paramagnetic liver cells were sorted, sequenced, and indexed according to the *C. livia* reference genome [*Cliv_1.0* reference genome (GCF_000337935.1)]; $n = 1$ pigeon. Fisher's exact test (significance determined as P_{adj} for multiple testing) was used to evaluate the probability of magnetic cells to be macrophages, dendritic cells, or B lymphocytes, on the basis of signature genes from the cellxgene.cziscience.com database. (**J**) Transcripts per million (TPM) of genes involved in erythrocyte clearance and iron metabolism, identified in sorted MHC II$^+$ cells. (**K**) Fluorescently labeled dextran (or nonlabeled dextran as vehicle control) was fed to isolated (magnetic) pigeon liver cells and human THP-1 cells (a monocyte-macrophage cell line) to estimate their phagocytic capacity. After 2 hours, cells were washed, fixed, and analyzed by flow cytometry. $n = 3$ or 4 independent experiments with THP-1 cells, and $n = 4$ independent experiments with isolated MHC II$^+$ pigeon cells. Data are shown as mean ± SEM.

of magnetic ferritin particles in tissue sections relative to sorted cells or purified ferritin. These magnetic signals, though modest, were 20 to 30 times higher than the magnetometer's noise level, which indicated an accumulation of iron and thus a substantial accumulation of nanomagnets in pigeon liver, and a much lower accumulation in the spleen. We verified this interpretation by demonstrating the presence of ferric iron with Prussian blue, which specifically stains ferric iron (Fe^{3+}) within ferritin proteins (*28*). A high number of Fe^{3+}-containing cells were seen in the liver and a few in the spleen, but none were observed in the brain, muscle, eye, or beak (Fig. 1D), consistent with results of the VSM analyses (Fig. 1, A to C).

Pigeon liver contains MHC II$^+$ macrophages that store Fe^{3+}

The morphology and localization of the iron-positive cells in the sinusoids of the hepatic portal triad suggested that these might be macrophages. Unfortunately, few antibodies exist that can identify pigeon cells with immunohistology. One of them identifies major histocompatibility complex class II (MHC II), which is expressed by antigen-presenting cells, including macrophages, dendritic cells, and B lymphocytes. We detected MHC II$^+$ cells in the same cellular localization and with the same morphology as Prussian blue–positive cells in pigeon liver (Fig. 1E) and confirmed colocalization by combining iron and MHC II staining, which yielded overlapping signals (Fig. 1F).

We next wanted to isolate these cells for further analysis by exploiting their ability to bind to magnetic columns as previously reported (*25*), and we indeed recovered magnetic liver cells from the columns (Fig. 1G). We also purified MHC II$^+$ cells by fluorescence-activated cell sorting (FACS) and performed 3′ mRNA sequencing (Fig. 1H). Sequencing reads were annotated using a publicly available *Columba livia* reference genome [*Cliv_1.0* reference genome (GCF_000337935.1)], which identified 7116 protein-coding genes. The expression profile of these cells was compared with mammalian macrophage signature genes from the cellxgene.cziscience.com database. We observed a significant overlap between our dataset and 43 macrophage signature genes [Fisher's exact test, adjusted P (P_{adj}) = 0.0321], whereas no significant overlap was detected for dendritic cell or B cell signatures (P_{adj} = 0.2461) (Fig. 1I). Because the macrophage, dendritic cell, and B cell gene sets contain both cell type–specific and shared markers, we performed two comparisons: one using only cell type–specific markers and one using the full marker sets. In both analyses, the macrophage signature showed significant enrichment in our isolated MHC II$^+$ cells, but the dendritic cell and B cell signatures did not.

Additionally, we found high expression of iron metabolism–related genes such as *Spi-c*, which encodes a transcription factor essential for red pulp macrophage development in the mammalian spleen (Fig. 1J). This suggested that the sorted MHC II$^+$ cells were involved in erythrocyte clearance and ferric iron and ferritin accumulation (*31*). Finally, we cocultured these cells with fluorescently labeled dextran and observed that they took it up nearly as efficiently as THP-1 cells (a human monocyte-macrophage cell line), which served as a positive control (Fig. 1K). Together, these findings confirmed that pigeon liver contains macrophages that accumulate iron, providing them with superparamagnetic properties.

Clodronate treatment depletes superparamagnetic cells in vivo

A defining feature of macrophages is their elimination after phagocytosis of clodronate liposomes, a widely used approach for macrophage depletion in vivo (*32*, *33*). Intravenous clodronate liposome administration depletes liver and spleen macrophages within 24 hours for up to 5 days, whereas peritoneal and lung macrophage depletion requires intraperitoneal injection and takes 3 days (*34*). To preferentially target pigeon liver macrophages, clodronate was administered intravenously 24 hours before analysis. After treatment, iron-containing hepatic cells were significantly (Student's t test, $P \leq 0.001$) reduced, supporting their macrophage identity, and residual iron staining appeared diffusely distributed, likely reflecting iron scavenging by hepatocytes (Fig. 2A). Consistently, magnetic cell separation failed to recover magnetic cells from clodronate-treated pigeon livers (Fig. 2B), which also showed a decrease in hepatic *Spi-c* expression (Fig. 2C) and fewer MHC II$^+$ cells (Fig. 2D). Clodronate treatment has been reported to affect neutrophil function (*35*). Although neutrophils are circulating and not classical tissue-resident immune cells, we wanted to exclude heterophils, the avian neutrophil equivalent (*36*), as candidate iron-positive cells. Heterophils were absent from liver tissue but detectable in blood smears, where they showed no iron accumulation (Fig. 2E). Moreover, polymorphonuclear cells isolated from blood (Fig. 2F) lacked magnetic blocking or hysteresis in VSM, displaying strictly linear magnetization behavior around zero field (Fig. 2G) and no magnetic blocking at low temperatures (compare with Fig. 1A) or hysteresis loops (compare with Fig. 1C), confirming the absence of ferrimagnetic properties of heterophils. Collectively, these results confirmed that the cells accumulating ferric iron in pigeon liver are macrophages.

Iron-positive macrophages are in proximity to hepatic nerve fibers

We next investigated how macrophages might transmit signals to the brain and hypothesized that innervation of hepatic sinusoids might mediate this communication. In mammals, hepatic nerve fibers traverse the sinusoids and frequently surround blood vessels and bile ducts, particularly within the portal triad (*37*, *38*) (Fig. 3A). Given the conserved architecture of the avian liver, we reasoned that similar neural structures would be present. Using Masson-Goldner staining, we identified nerve bundles embedded within green-stained collagenous connective tissue of the portal triad (Fig. 3B). These bundles were characterized by their wavy fiber texture in pale red with elongated Schwann cell nuclei, in contrast to dark, densely red-stained hepatocytes in the surrounding tissue. Additionally, we used silver staining to specifically stain for nerve fibers. We identified neurons in pigeon brain (used as positive control; fig. S1C) and peripheral nerve fibers in liver tissue (Fig. 3C). Prussian blue staining of sequential tissue slides showed the presence of iron-positive macrophages in the same area. After clodronate treatment, these associations were no longer observed. To further assess macrophage-nerve interactions, we performed electron microscopy. We identified bundles of unmyelinated axons containing neurofilaments, visible as small puncta in cross sections or as fine elongated filaments in longitudinal sections (fig. S1A), as well as large mitochondria and neurotransmitter vesicles, which are indicative of nerve bundles of the autonomic nervous system. Macrophages were identified by their heterogeneous, irregularly shaped nucleus and cytoplasm rich in mitochondria, lysosomes, and intracellular vesicles and vacuoles (fig. S1B). We found macrophages frequently located in proximity (≤2 μm) to nerve fibers, allowing for paracrine signaling or direct cell-cell contact. After clodronate treatment, the few remaining macrophages displayed apoptotic-like morphology, marked by numerous membrane-bound phagolysosomal vacuoles, altered mitochondria, and condensed nuclei, whereas nerve structures remained intact (Fig. 3D and fig. S1D). Overall, these images confirmed a close spatial relationship between macrophages and nerve fibers, suggesting their potential interaction.

Temporary macrophage depletion in pigeons impairs their homing orientation and navigation

Under completely overcast conditions, when the sun and polarized light cues are unavailable and visual landmarks are obscured, homing pigeons rely on their magnetic sense (*39*–*41*) [and see (*42*, *43*) for ongoing debate in this field]. To explore whether superparamagnetic macrophages contribute to pigeons' navigation, we performed clodronate depletion in living pigeons.

Thirty-four pigeons were trained individually to home over a 19-km route from west to east. After 10 successful training flights, birds were randomized to receive either intravenous clodronate liposomes (n = 18)

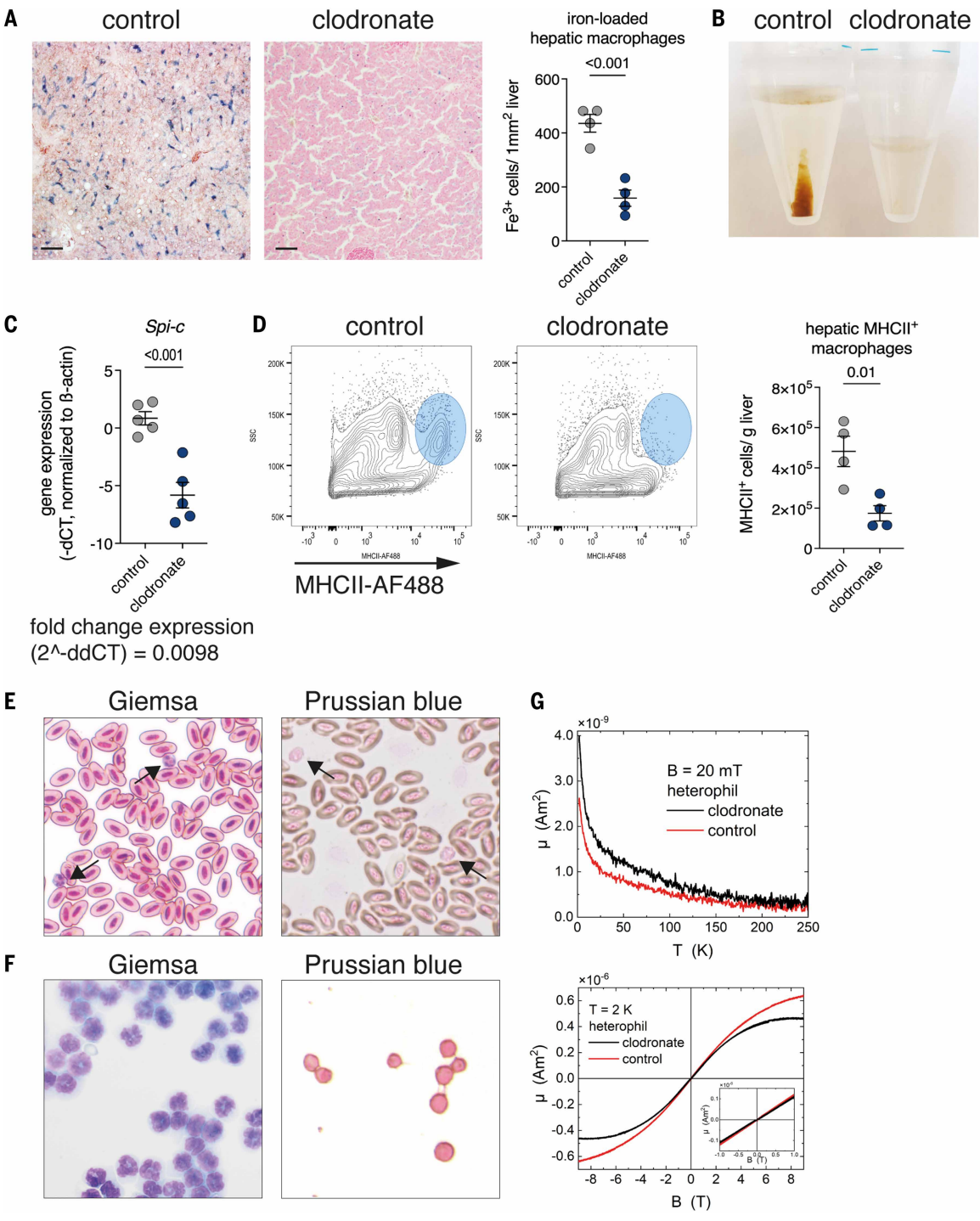

Fig. 2. Effect of clodronate treatment on hepatic macrophages and peripheral heterophils. (**A**) Pigeons were treated with clodronate or control liposomes and sacrificed 24 hours later. Representative histological images of iron staining of liver tissue from control (see also Fig. 1D) and clodronate-treated pigeons. Scale bars are 100 μm. Iron-loaded cells were manually counted by microscopy per 1 mm^2 of liver tissue. Four independent experiments were performed, and for each, the mean of two technical replicates is shown. (**B**) Representative photo of hepatic cells isolated by a magnetic column from control and clodronate-treated pigeons. (**C**) Gene expression of *Spi-c* in the liver tissue of control or clodronate-treated pigeons. (**D**) Representative flow cytometry plots and quantification of MHC II^+ cells in liver tissue from control and clodronate-treated pigeons. (**E**) Representative bright-field microscopy images of pigeon blood smears stained with Giemsa or Prussian blue showing nucleated erythrocytes and heterophils (black arrows), the avian equivalent of mammalian neutrophils. (**F**) Polymorphonuclear cells isolated by density gradient centrifugation from pigeon blood, stained with Giemsa or Prussian blue. (**G**) Vibrating sample magnetometry as function of temperature *T* at *B* = 20 mT (top) and induction *B* at *T* = 2 K (bottom). The inset indicates a strictly paramagnetic (linear) field dependence without hysteresis around zero field. For quantification in (A), (C), and (D), unpaired two-tailed Student's *t* test was used to determine statistical significance. Data are from independent experiments and presented as mean ± SEM.

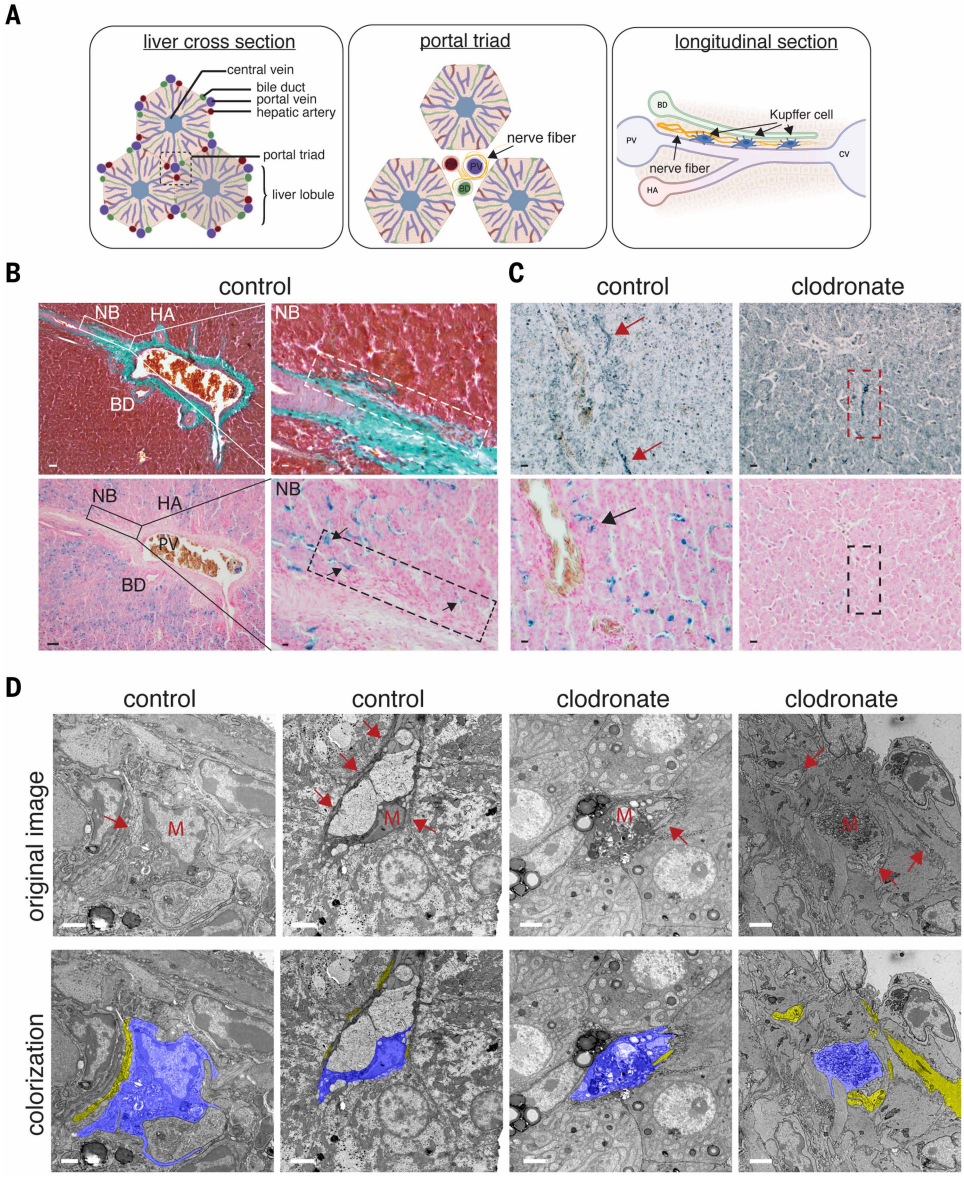

Fig. 3. Iron-positive macrophages and nerve fibers in the pigeon liver. (**A**) Schematic liver anatomy. On the left is a cross section showing three liver lobules and the portal triad containing branches of portal vein, bile duct, and hepatic artery. In the middle is a portal triad showing nerve branches around blood vessels and the bile duct. On the right is a longitudinal section depicting the portal vein, central vein, bile duct, and hepatic artery, as well as nerve fibers and Kupffer cells. [Figure created with BioRender.com] (**B**) Sequential cross sections of pigeon liver tissue stained with Masson-Goldner (top) or Prussian blue (bottom). The left column shows a region surrounding a portal vein (PV), including bile duct (BD) and hepatic artery (HA). Boxes highlight a nerve bundle (NB) embedded in connective tissue (green). Scale bars are 50 μm. The right column is a magnification of the nerve bundle. The black arrow indicates an association between nerve fibers and macrophages. Scale bars are 10 μm. (**C**) Sequential cross sections of pigeon liver tissue stained with silver for nerve fibers (top) or Prussian blue (bottom) for iron-positive macrophages. Red arrows indicate nerve fibers in proximity to vessels. Black arrows indicate iron-positive macrophages in the same area. Dashed boxes indicate a nerve in clodronate-treated liver (top) and the corresponding area with Prussian blue staining (bottom). Scale bars are 10 μm. (**D**) Electron microscopy of liver tissue from control and clodronate-treated pigeons. The top row shows the original images, with red arrows indicating nerve fibers and "M" indicating a macrophage. The bottom row shows pseudo-colorization of the images, where yellow indicates nerve bundles and blue indicates macrophages. Scale bars are 2 μm.

or control liposomes ($n = 16$) (Fig. 4A) when the weather forecast predicted completely overcast conditions for the next day. Twenty-four to 28 hours later, pigeons were released individually under completely overcast conditions and tracked using real-time Internet of Things GPS devices (*44*, *45*) (Fig. 4B). All control-treated pigeons homed within 70 min, whereas none of the clodronate-treated birds returned on the same day under persistent overcast conditions, instead displaying random spatial orientation (Fig. 4, C to E). Importantly, macrophage-depleted pigeons homed normally once cloud cover cleared and the sun became visible, indicating intact flight capacity, motivation, and overall health. When we retreated control pigeons with clodronate, they successfully homed under sunny conditions (i.e., when directional solar information is available), with high track efficiency, similar to their prior performance (Fig. 4F). Together, these findings indicated that pigeons can sense magnetic direction independent of a purported visual (cryptochrome-mediated) magnetic sensing system and that macrophages are required for finding magnetic direction under conditions in which solar and landmark cues are unavailable.

Discussion

Three principal theories for magnetoreception in pigeons have been proposed to date. Our findings support a fourth mechanism, on the basis of the collective sensing capacity of superparamagnetic macrophages, located predominantly in the liver, that enables perception of geomagnetic direction. Drawing on established macrophage-neuron communication pathways (*46*, *47*), we propose that hepatic macrophages sense changes in Earth's magnetic field and transmit this information to the brain via afferent vagal innervation. We posit that magnetic sensing requires a cell population–level signal, rather than single-cell detection, to reach the threshold for neuronal activation. Liver macrophages are well equipped for this role, as they accumulate ferric iron during erythrocyte clearance and are closely associated with autonomous nerves. Such nerves, for example, the vagus or sympathetic nerves, generally provide rapid, bidirectional communication between peripheral organs and the brain and are ideally positioned to relay magnetic information sensed in the liver (*48*).

At the cellular level, we propose that ferritin-bound unpaired electrons interact through magnetic dipole-dipole coupling, which increases collective magnetic susceptibility, enabling uniform alignment along Earth's declination lines. This process may be functionally analogous to magnetosomes in magnetotactic bacteria that drag prokaryotic cells along the magnetic field (*49*). The characteristic circling behavior observed in pigeons after take-off (*50*) may facilitate the imprinting of the magnetic information of electrons in ferritin particles in a uniform manner before directed flight. Such alignment is likely to induce changes in intracellular organization or

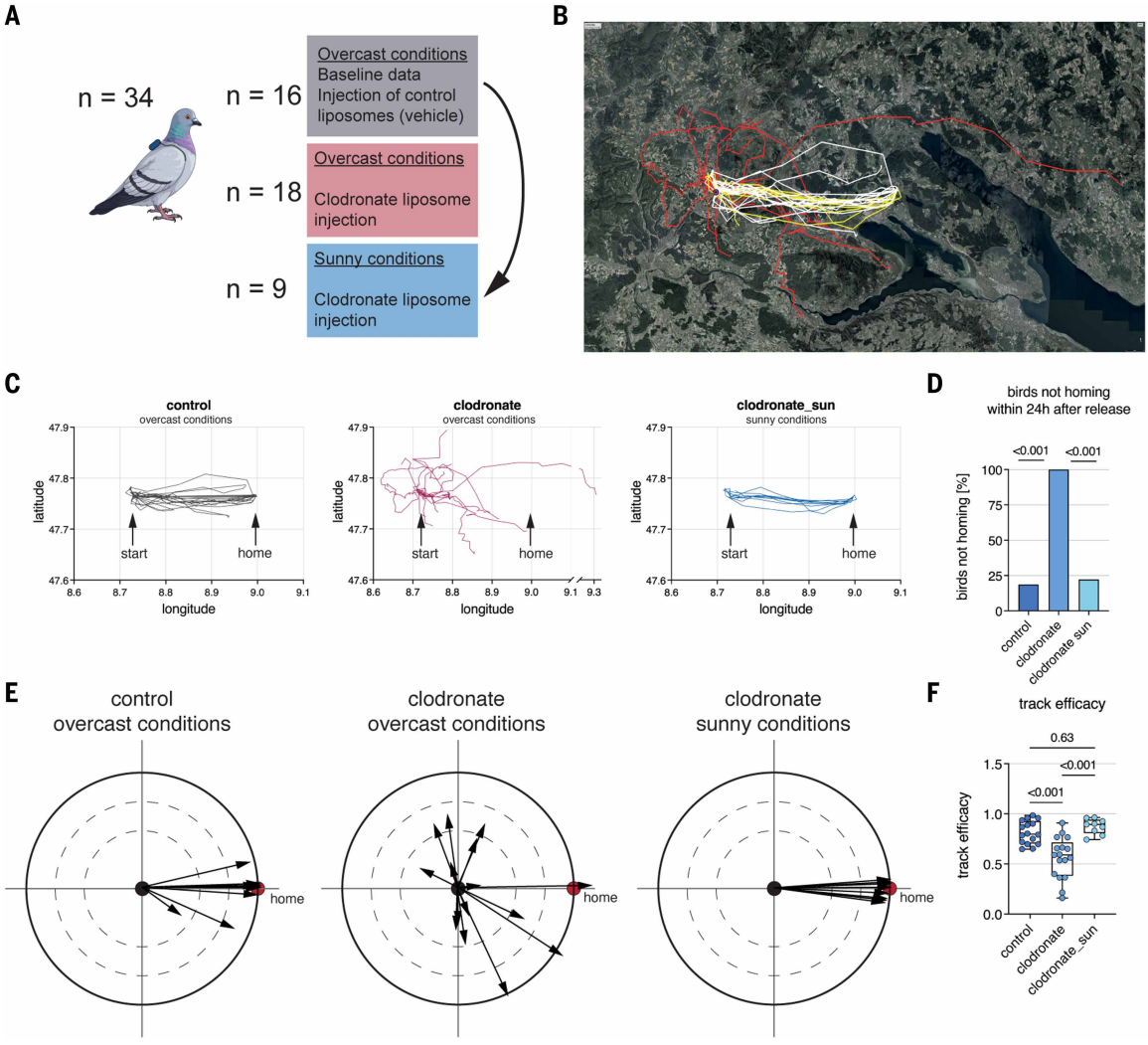

Fig. 4. Effect of clodronate treatment on pigeon navigation. (**A**) Pigeons ($n = 34$) were trained to return home from west to east. One day before inclement weather conditions (completely overcast, during a total of six experimental days across 2 years), the pigeons were intravenously treated with 0.5 ml of clodronate ($n = 18$) or control liposomes ($n = 16$). (**B**) After 24 to 28 hours, the pigeons were released 19 km from home and tracked by GPS (white indicates control birds, $n = 16$; red indicates clodronate-treated birds, overcast conditions, $n = 18$; yellow indicates clodronate-treated birds, sunny conditions, $n = 9$). (**C**) Pigeon tracks of the three experimental groups depicted separately. Each line represents one pigeon. (**D**) Most of the pigeons in the control and clodronate sun groups returned home on the experimental day, whereas none of the clodronate-treated birds managed to do so on the overcast day of release. (**E**) GPS data within 95 min after take-off were transformed into vectors resembling flight trajectories for all groups. Arrows represent the flight direction of each pigeon, and their length corresponds to the aerial distance covered within the 95 min, showing that pigeons in the clodronate group exhibited reduced navigational efficiency, as they covered considerable distances but in a less directed manner. (**F**) Track efficacy of control or clodronate-treated pigeons (sunny and overcast conditions), calculated as the aerial distance from release site to home divided by the total distance traveled to reach home (within the 95 min of measurement), where 1 indicates perfect efficiency (the bird traveled in a straight line) and 0 indicates least efficiency. Data were analyzed by one-way analysis of variance (ANOVA) with Tukey's honest significant difference post hoc test. Data are presented as box plots showing median (line), 25th to 75th percentiles (box), and minimum-maximum values (whiskers).

polarization within hepatic macrophages (*51*), consistent with known macrophage responses to mechanical stimuli (*52*). Acting as a coordinated array, macrophages could transmit magnetic information to nearby nerve afferents through spatial summation, either through direct mechanical coupling (*53*), analogous to baroreceptor signaling (*54*) and similar to other vertebrate sensing and induction systems such as peripheral macrophage-to-sensory redox cross-talk (*55*), or through paracrine release of soluble mediators, an established macrophage-nerve signaling mechanism (*56*). The brain would then integrate this magnetic input with other sensory cues to compute spatial orientation, for example, in the pallial regions in the brain, as suggested recently (*24*).

A strength of our model is its potential to also explain magnetoreception in animals that lack functional cryptochromes or operate in environments with little to no light, including bats (*57*, *58*) and blind mole rats (*59*). Additionally, elasmobranchs such as sharks can detect variations in the geomagnetic field (*60*), and tiger sharks (*61*), blue sharks (*62*), and scalloped hammerhead sharks swim in straight lines over long distances, with the latter even orienting toward seamounts associated with geomagnetic anomalies (*63*). Beyond magnetoreception, our findings contribute to a broader emerging concept: Tissue-resident macrophages can function as peripheral sensory cells, providing direct, biologically meaningful feedback to the brain (*25*, *47*, *64*).

REFERENCES AND NOTES

1. U. Demšar, B. Zein, J. A. Long, *Mov. Ecol.* **13**, 16 (2025).
2. A. M. Berdahl *et al.*, *Philos. Trans. R. Soc. London Ser. B* **373**, 20170009 (2018).
3. C. Walcott, *Integr. Comp. Biol.* **45**, 574–581 (2005).
4. K. Thorup, R. A. Holland, A. P. Tøttrup, M. Wikelski, *Integr. Comp. Biol.* **50**, 315–322 (2010).
5. W. W. Cochran, H. Mouritsen, M. Wikelski, *Science* **304**, 405–408 (2004).
6. R. Muheim, J. B. Phillips, S. Akesson, *Science* **313**, 837–839 (2006).
7. R. C. Beason, W. Wiltschko, *J. Comp. Physiol. A Neuroethol. Sens. Neural Behav. Physiol.* **201**, 961–967 (2015).
8. W. Hodos, A. B. Butler, *Brain Behav. Evol.* **50**, 189–197 (1997).
9. W. T. Schneider, R. A. Holland, O. Lindecke, *Eur. Phys. J. Spec. Top.* **232**, 269–278 (2023).
10. R. Wiltschko, W. Wiltschko, *J. R. Soc. Interface* **16**, 20190295 (2019).
11. G. Fleissner, B. Stahl, P. Thalau, G. Falkenberg, G. Fleissner, *Naturwissenschaften* **94**, 631–642 (2007).
12. B. Zein *et al.*, *Mov. Ecol.* **9**, 46 (2021).
13. L. Tian *et al.*, *Biometals* **20**, 197–203 (2007).
14. H. G. Hiscock *et al.*, *Proc. Natl. Acad. Sci. U.S.A.* **113**, 4634–4639 (2016).
15. K. M. Goforth *et al.*, *Nature* **638**, 1015–1022 (2025).
16. T. Hochstoeger *et al.*, *Sci. Adv.* **6**, eabb9110 (2020).
17. P. J. Hore, H. Mouritsen, *Annu. Rev. Biophys.* **45**, 299–344 (2016).
18. H. Mouritsen, *Nature* **558**, 50–59 (2018).
19. D. Timmer *et al.*, *J. Am. Chem. Soc.* **145**, 11566–11578 (2023).
20. S. T. Emlen, J. T. Emlen, *Auk* **83**, 361–367 (1966).
21. F. Nievergelt, F. Liechti, *J. Ornithol.* **141**, 389–389 (2000).
22. C. D. Treiber *et al.*, *Nature* **484**, 367–370 (2012).
23. D. J. Panagopoulos, A. Karabarbounis, G. P. Chrousos, *Sci. Rep.* **14**, 30053 (2024).
24. G. C. Nordmann *et al.*, *Science* **391**, 1155–1160 (2026).
25. L. Franken *et al.*, *Sci. Rep.* **5**, 12940 (2015).
26. T. Korolnek, I. Hamza, *Blood* **125**, 2893–2897 (2015).
27. T. R. L. Klei *et al.*, *Blood* **136**, 1579–1589 (2020).
28. N. D. Chasteen, P. M. Harrison, *J. Struct. Biol.* **126**, 182–194 (1999).
29. P. Arosio, L. Elia, M. Poli, *IUBMB Life* **69**, 414–422 (2017).
30. S. A. Makhlouf, F. T. Parker, A. E. Berkowitz, *Phys. Rev. B* **55**, R14717–R14720 (1997).
31. M. P. Soares, I. Hamza, *Immunity* **44**, 492–504 (2016).
32. N. van Rooijen, E. Hendrikx, in *Liposomes:Methods and Protocols*, vol. 1, Methods in Molecular Biology Series, V. Weissig, Ed. (Springer, 2010), pp. 189–203.
33. H. D. Danenberg *et al.*, *Circulation* **106**, 599–605 (2002).
34. N. Van Rooijen, A. Sanders, *J. Immunol. Methods* **174**, 83–93 (1994).
35. S. Culemann *et al.*, *J. Exp. Med.* **220**, e20220525 (2023).
36. K. J. Genovese, H. He, C. L. Swaggerty, M. H. Kogut, *Dev. Comp. Immunol.* **41**, 334–340 (2013).
37. B. M. Miller, I. M. Oderberg, W. Goessling, *Hepatology* **74**, 3513–3522 (2021).
38. H. R. Berthoud, H. Münzberg, C. D. Morrison, W. L. Neuhuber, *Auton. Neurosci.* **253**, 103174 (2024).
39. W. T. Keeton, *Proc. Natl. Acad. Sci. U.S.A.* **68**, 102–106 (1971).
40. M. M. Walker, *J. Theor. Biol.* **192**, 341–349 (1998).
41. W. Wiltschko, R. Wiltschko, *J. Avian Biol.* **48**, 66–74 (2017).
42. C. Walcott, *J. Exp. Biol.* **199**, 21–27 (1996).
43. R. Holland, C. Filannino, A. Gagliardo, *J. Exp. Biol.* **216**, 2192–2200 (2013).
44. T. A. Wild *et al.*, *Anim. Biotelemetry* **11**, 13 (2023).
45. A. Gagliardo, P. Ioalè, C. Filannino, M. Wikelski, *PLOS ONE* **6**, e22385 (2011).
46. A. J. Shepherd *et al.*, *J. Neurosci.* **38**, 7032–7057 (2018).
47. M. Hulsmans *et al.*, *Cell* **169**, 510–522.e20 (2017).
48. L. Ma, H. B. Wang, K. Hashimoto, *Brain Behav. Immun.* **124**, 28–39 (2025).
49. R. Blakemore, *Science* **190**, 377–379 (1975).
50. A. Gagliardo, E. Pollonara, M. Wikelski, *Ethol. Ecol. Evol.* **33**, 321–337 (2021).
51. J. L. Rohn, B. Baum, *J. Cell Sci.* **123**, 155–158 (2010).
52. S. Adams, L. M. Wuescher, R. Worth, E. Yildirim-Ayan, *Ann. Biomed. Eng.* **47**, 2213–2231 (2019).
53. M. A. Freitas-Lopes, K. Mafra, B. A. David, R. Carvalho-Gontijo, G. B. Menezes, *Cells* **6**, 48 (2017).
54. J. M. Karemaker, *Biol. Psychol.* **172**, 108378 (2022).
55. A. J. Shepherd *et al.*, bioRxiv, 166546 (2017).
56. R. Dantzer, J.-P. Konsman, R.-M. Bluthé, K. W. Kelley, *Auton. Neurosci.* **85**, 60–65 (2000).
57. R. A. Holland, K. Thorup, M. J. Vonhof, W. W. Cochran, M. Wikelski, *Nature* **444**, 702 (2006).
58. R. A. Holland, J. L. Kirschvink, T. G. Doak, M. Wikelski, *PLOS ONE* **3**, e1676 (2008).
59. T. Kimchi, J. Terkel, *J. Exp. Biol.* **204**, 751–758 (2001).
60. C. G. Meyer, K. N. Holland, Y. P. Papastamatiou, *J. R. Soc. Interface* **2**, 129–130 (2005).
61. C. G. Meyer *et al.*, *Sci. Rep.* **8**, 4945 (2018).
62. F. Vandeperre *et al.*, *PLOS ONE* **9**, e103538 (2014).
63. A. P. Klimley, *Mar. Biol.* **117**, 1–22 (1993).
64. X. Yu *et al.*, *Nat. Commun.* **11**, 264 (2020).

ACKNOWLEDGMENTS

We thank the animal caretakers at the Max Planck Institute of Animal Behavior (MPIAB) for training and maintaining the pigeons and the MPIAB Wild Lab, as well as G. Heine and the University of Konstanz Technical Workshop for providing GPS tracking systems. We thank the Flow cytometry Core Facility of the Medical Faculty at the University of Bonn for providing support and instrumentation funded by the Deutsche Forschungsgemeinschaft (DFG, German Research Foundation) and for funding a BD LSR Fortessa and AriaIII cell sorter. We also thank the Microscopy Core Facility of the Medical Faculty at the University of Bonn for providing instrumentation funded by the DFG (project no. 388171357) and the Next Generation Sequencing Core Facility of the University Hospital Bonn. We thank S. Härtle from Ludwig Maximillian University of Munich for discussions on pigeon-specific antibodies and D. Legler for discussions on macrophage functionality. We also thank B. Rau and M. Michels for technical assistance. **Funding:** This work was supported by the Max Planck Society, the Gordon and Betty Moore Foundation grant GBMF10539, and the Academy for the Protection of Zoo Animals and Wildlife to M.W.; by the DFG consortia SFB1454, IRTG2168, TRR237, TRR259, SFB1540, FOR5427, EXC2151, EXC 2047, TRR270; by a Schlegel Professorship to J.H.; and by a Gottfried Wilhelm Leibniz Award to C.K. **Author contributions:** Conceptualization: C.K., M.W.; Funding acquisition: M.W., U.W., M.F., C.K.; Investigation and methodology: C.L., M.Q., D.K., L.L., L.S., M.G., J.L., I.M., D.Z., U.W., M.W., S.K., L.F.; , J.H., K.T., W.F., D.K.N.D. Project management: C.L., M.Q., M.W., C.K.; Supervision: C.L., M.W., C.K.; Writing – original draft: C.L., U.W., C.K., M.W.; Writing – review & editing: All authors. **Competing interests:** The authors declare that they have no competing interests. **Data, code, and materials availability:** All pigeon tracking data will be available in the Movebank Data Archive (movebank.org) upon publication. 3′ mRNA sequencing data of MHC II$^+$ cells isolated from liver homogenate will be available on the European Nucleotide Archive (ENA) database (accession no. PRJEB98986) upon publication. This research was funded in whole or in part by the DFG (216372401, 216372545, 272482170, 369799452, 387335189, 388171357, 390685813, 390873048, 397484323, 432325352, 405553726, 460333672, 466687329, and 60333672); as required, the author will make the Author Accepted Manuscript (AAM) version available under a CC BY public copyright license.

SUPPLEMENTARY MATERIALS

science.org/doi/10.1126/science.ady2486
Materials and Methods; Fig. S1; References; MDAR Reproducibility Checklist

Submitted 15 April 2025; accepted 31 March 2026

10.1126/science.ady2486

Homing pigeon navigation relies on superparamagnetic macrophages under overcast conditions

Clivia Lisowski, Michael Quetting, Daniela Klaus, Lisa Lazarevski, Lea Seep, Maximilian Germer, Jian Li, Inge Müller, Daniel Zuniga, Wolfgang Fiedler, Dina K. N. Dechmann, Kasper Thorup, Jan Hasenauer, Lars Fester, Stefanie Kuerten, Michael Farle, Ulf Wiedwald, Martin Wikelski, and Christian Kurts

Science **392** (6801), . DOI: 10.1126/science.ady2486

Editor's summary

It has long been known that birds rely, at least in part, on magnetoreception to orient their movements. The mechanisms underlying this reception appear to be numerous and are still being discovered. Physiological connections have been found in the head, including the beak, eyes, and brain, but Lisowski *et al.* have now identified the presence of superparamagnetic macrophages in the liver (see the Perspective by Spiro and Drakesmith). On cloudy days when they could not see the sun, pigeons whose magnetic macrophages had been depleted were unable to navigate home. The authors conclude that these liver-based macrophages are required for navigation when the sun doesn't shine. — Sacha Vignieri